Clays and Clay Minerals, Vol. 50, No. 6, 807–823, 2002.

DIAGENESIS AND RHEOLOGY OF A RECENT–PLEISTOCENE VOLCANOGENIC SEDIMENTARY SEQUENCE, MEXICAN BASIN

LIBERTO DE PABLO-GALÁN[1,*], JUAN J. DE PABLO[2] AND M. DE LOURDES CHÁVEZ-GARCÍA[3]

[1] Instituto de Geología, Universidad Nacional A. de Mexico, 04510 Mexico, D.F.
[2] Chemical Engineering Department, University of Wisconsin, Madison, Wisconsin, USA
[3] Facultad de Química, Universidad Nacional A. de Mexico, 04510 Mexico, D.F.

Abstract—Diagenesis of the Holocene-Pleistocene volcanogenic sediments of the Mexican Basin produced, in strata of gravel and sand, $1H_2O$- and $2H_2O$-smectite, kaolinite, R3-$2H_2O$-smectite (0.75)-kaolinite, R1-$2H_2O$-smectite (0.75)-kaolinite, R3-kaolinite (0.75)-$2H_2O$-smectite and R1-$1H_2O$-smectite (0.75)-kaolinite. Smectite platelets were formed from volcanic glass by loss of Si^{4+}. Partially-formed platelets have Si^{4+} between 4.55–4.10 a.p.f.u., Mg+Mn and the interlayer charge are relatively uniform while $^{VI}Al+Fe^{3+}+Ti$ varies between 0.98 and 1.63 a.p.f.u. Almost fully transformed platelets have Si^{4+} of 4.08–4.04 a.p.f.u.; Mg+Mn and the interlayer charge decrease proportionally to increasing $^{VI}Al+Fe^{3+}+Ti$. Smectite-kaolinite mixed layers have octahedral occupancies of 2.01–2.15 a.p.f.u., $^{IV}Al^{3+}$ 0.09–0.55 a.p.f.u. and interlayer charges about half that of smectite; structural formulae corresponding to smectite (0.75–0.80)-kaolinite indicate octahedral occupancy of 2.50 a.p.f.u., tetrahedral replacement 0–0.31 a.p.f.u., and interlayer charge 0.24–0.51 equivalents, some indicating interstratifications of beidellite. Kaolinite is presumed to have formed from K-feldspar; smectite-kaolinite interstratifications sustain the transformation of kaolinite to smectite in an increasingly siliceous high-cation environment. In the mudstones of low-hydraulic conductivity and practically stagnant alkaline fluids, glass was transformed to $2H_2O$-smectite lamellae of ^{IV}Al between 0 and 0.47 a.p.f.u., octahedral occupancy 1.70–2.00 a.p.f.u. and interlayer charge of 0.23–1.21 equivalents, some corresponding to beidellite. The interlayer charge increases with ^{IV}Al and decreasing occupancy of the octahedral sheet; the abundance of Mg+Mn is inverse to that of $^{VI}Al+Fe^{3+}+Ti$.

Clay suspensions containing $1H_2O$- and $2H_2O$-smectite, kaolinite and R3-$2H_2O$-smectite (0.75)-kaolinite lead to low-energy edge-to-edge particle associations, non-Newtonian pseudoplastic behavior, and maximum apparent viscosity of 180 Pa s at 0.008 s^{-1} followed by rapid descent. Clay fractions with slightly larger $2H_2O$-smectite contents and smaller kaolinite contents reach maximum viscosity of 3611 Pa s at a shear rate of 0.0018 s^{-1} and of 3300 Pa s at 0.0024 s^{-1}. They denote two high-energy face-to-face particle associations, followed by slow descent of the apparent viscosity under viscous flow. Suspensions change from elastic to viscous behavior at shear stresses of 1.03 and 5.91 Pa, respectively. Clay suspension vibrated at a frequency of 1 Hz develops a shear storage dynamic modulus greater than the shear dynamic loss modulus or the energy is preferentially stored, whereas at 5 Hz more energy is dissipated than stored.

Key Words—Clay Mineralogy, Diagenesis, Recent Volcanogenics, Mexican Basin, Rheology.

INTRODUCTION

Young volcanogenic sediments form mudrocks characterized by physical and chemical instability. Their patterns of failure when under load frequently point to non-uniform behavior that could be related to their mineralogy and diagenesis. In older sediments, which would normally be stable, diagenesis forms trioctahedral smectite, Mg-rich chlorite, interstratified chlorite-smectite and corrensite (Kübler, 1973; Kopp and Fallis, 1974; Furbish, 1975; Almon *et al*., 1976; April, 1981; Pevear and Whitney, 1982; Chang *et al*., 1986; Bodine and Madsen, 1987; Inoue and Utada, 1991; Hillier 1993; Jiang and Peacor, 1994; Barrenechea *et al*., 2000). Between the low-temperature smectite and the high-temperature chlorite there is a sequence of interstratified chlorite-smectite and corrensite (Hutcheon *et al*., 1980; Meunier *et al*., 1988; Hillier, 1993; Jiang and Peacor, 1994; Jiang *et al*., 1994). The transformation of smectite to corrensite to chlorite has been described as continuous, characterized by random and regular interstratifications (April, 1981; Bettison-Varga and Mackinnon, 1997), and as a series of discontinuous steps (Shau *et al*., 1990; Hillier and Velde, 1991; Hillier, 1993; Schiffman and Staudigel, 1995; Roberson, 1989).

Diagenesis in young sediments has not been so completely documented, although the transformation of volcanogenic sediments to smectite is known. Various 7 Å-layer minerals may occur with smectite, some of which have been loosely referred to as 7 Å chlorite, serpentine-like 7 Å layers, 7 Å layer or 7 Å clay (Jiang *et al*., 1994; Karpova, 1969). Karpova (1969) described an Fe-7 Å chlorite *Ib*($\beta = 90°$) that transforms to Fe-14 Å chlorite *Ib*($\beta = 90°$) to Mg-Fe 14 Å chlorite *IIb* by burial diagenesis, in terrigenous Carboniferous rocks. This Fe 7 Å chlorite could possibly be a high-Fe 14 Å chlorite or

* E-mail address of corresponding author:
liberto@servidor.unam .mx

any of the 7 Å high-Fe minerals chamosite, berthierine or even odinite (Brindley, 1982; Bailey, 1988a,b; Bailey and Brown, 1982; Odin, 1985; Odin *et al*., 1988). It could be presumed that, as in the case of trioctahedral smectite, diagenesis to 7 Å layer minerals or to dioctahedral smectite could be associated with interstratified minerals of 7 Å layer-smectite, chlorite-smectite or even with chlorite, distinct from those developed under more intense stages of diagenesis. A logical conclusion would be to expect dissimilar mechanisms of diagenesis and mineral assemblages within the pores and channels of the coarse ash and sand, and in the less permeable fine ash and mudstones. From the point of view of physical and chemical stability, it would not be expected that the minor occurrence of 7 Å layer minerals would modify significantly the behavior of the sediments, which would still depend on their principal clay component, smectite. Based on the anomalous behavior of young sediments, it may be postulated that variations in the precursor minerals or in their diagenesis would result in distinct clay minerals, unevenly distributed through a sedimentary sequence with non-uniform physical behavior. Management of the stability of the sediments would require knowledge of their variation.

This paper will document the occurrence and distribution of clay minerals, and diagenesis in the volcanogenic sediments of the Recent-Pleistocene depositional sequence of the Mexican Basin, Central Mexico, and the significance of their physical behavior, characterized by their shear rheology.

GEOGRAPHIC AND GEOLOGIC SETTING

The Mexican Basin extends between 19º00′ and 20º15″ N latitude and 98º15′ and 99º33′ W longitude, covering an area of 7160 km^2 in central Mexico (Figure 1). The Basin was formed in the Middle Tertiary when active volcanism developed thick sequences of basaltic andesite, andesite, dacite and latite (dacitic and rhyolitic lavas of Cerro del Chiquihuite, andesite flows of Sierras Nevada and Las Cruces, andesitic series of Ixtlacihualt and Ajusco). Volcanic activity decreased towards the end of the Miocene. Tectonism associated with the Clarion fault disrupted the crust along NNW–SSE fractures (Mooser, 1956a,b). In the Pliocene, high rainfall created the abrupt relief of the Middle and Upper Tertiary volcanic complexes and resulted in extensive fluvial deposits intercalated with strata of siltstone, lava flows and tuffs (Tarango Formation). During the Pleistocene the climate was humid and cold (Mooser, 1956a,b; Lopez-Ramos, 1979), glaciers developed in the Ixtlacihualt and Popocatepetl and large portions of the Tarango Formation were destroyed. The area was covered with thick layers of basalt and pumices (Chiconautla, Chimalhuacan and Estrella) until intense lava effusions, 2000 m thick, from the Chichinautzin closed the drainage at the south end of the Basin. This was followed by extensive deposition of air- and water-transported ashes that settled in the low areas (Tacubaya Formation). The formation is characterized by intercalated strata of pyroclastic sands, thin layers of sands with calcite and ashes that in the lacustrine environment were transformed to the high-swelling clays common to the Basin. Overlying the Tacubaya Formation are the lacustrine sediments of the Becerra Formation. The final eruptions were those of the Xitli ~2400 years ago and of the Popocatepetl in 1920 (Mooser, 1956a,b; Gasca and Reyes, 1977; Lopez-Ramos, 1979; Sistema Hidraulico del Distrito Federal, 1994).

A simplified stratigraphic column of the Mexican Basin, which will be referred as the Basin, shows a randomly distributed layered sequence of silt, mud, sand and gravel. The thickness of the mud in the Becerra

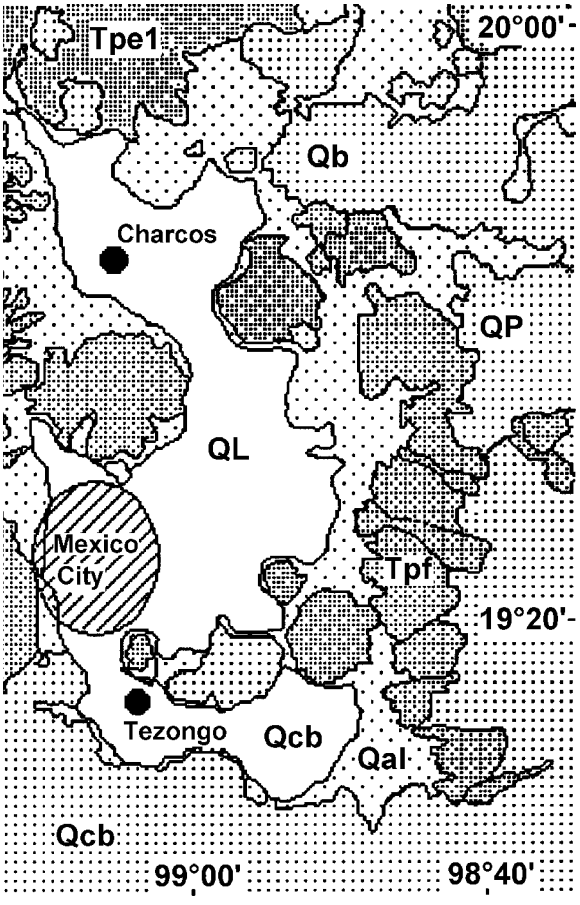

Figure 1. Geological map of the Mexican Basin. QL, Quaternary lacustrine deposits; Qal, Quaternary alluvial deposits; Qcb, Quaternary lavas and tuffs of the Chichinautzin Group, basaltic; Qb, Quaternary recent lavas; QP, Quaternary Pliocene basaltic lavas and tuffs older than the Chichinautzin Group; Tpf, Tertiary volcanic fans of the Tarango Formation; Tpel, Tertiary tuffaceous and pumice-rich soils (from Mooser, 1956; Sistema Hidraulico del Distrito Federal, 1994).

Formation varies. It is ~100 m in the southeast areas of Xochimilco and Chalco and northeast of Texcoco, whereas to the northwest, in Atcapotzalco, it ranges from 60 to 100 m, and in the remaining areas is 40 to 60 m thick. The sediments to be described are from locations north (Charcos) and south (Tezonco) of the Basin, in the Becerra and Tacubaya Formations (Figure 1).

The mud retains large amounts of water, forms gels that liquefy easily, is mechanically unstable, highly compressible and swells substantially (Marsal and Mazari, 1962). Other studies have described the hydrogeology (Durazo and Farvolden, 1989), stratigraphy and paleoenvironment of the southeastern part of the Basin (Urrutia *et al.*, 1994) and the distribution of heavy metals (Ruiz-Fernandez, 1999). The clay has been described as bentonitic but its mineralogy, swelling, instability and other properties have not been adequately resolved. It is the purpose of this paper to establish the clay mineral content and diagenesis and their possible influence on the physical and chemical stability of the sediments, particularly on their mechanical and adsorptive behavior.

SAMPLING AND METHODOLOGY

Samples were obtained from more than 20 drillholes extended over the Basin down to depths of 324 m. Two holes (Figure 1), located in the north (Charcos) and south (Tezonco) areas of the Basin and represented by 155 samples each, and 17 were chosen to illustrate the mineralogical details. They are black to brown mudstones with >85 wt.% clay and gravels and sands with volcanoclastic gravel-size fragments, lapilli, sand and ash and ~3–20 wt.% clay. The average properties of the mudstones were reported to be: water content 400 wt.%, liquid limit 1–70, plastic limit 30–80, cation exchange capacity 70 meq/100 g, deformation modulus 10.60 k/cm^2 when containing 50–600 wt.% water, and compressive modulus 2–8 k/cm^2 (Marsal and Mazari, 1962).

The samples were prepared by ultrasonic dispersion in deionized water, screening and sedimentation of the fine silt and sand. The concentration of clay minerals ranged between 3 and 85 wt.% of the bulk material, which, in cases, restricted the availability of clay for oriented slide preparation. Additionally, the strong gelling of the clay made it practically impossible to separate completely the very fine ash even after dilution, prolonged settling, centrifugation and dispersion with sodium hexametaphosphate. The <0.5 μm fraction, used for the rheology studies, was separated by gravity settling and successive centrifugation of the non-clay components, without adding any chemicals. The <0.5 μm fraction, used for the clay mineral analyses, was prepared by dilution to a solid to water ratio of 1/20 and prolonged settling for 150 h followed by centrifugation to concentrate the suspension.

Samples for X-ray diffraction (XRD) studies were prepared by dropping a few drops at a time of the thin supernatant suspensions on glass slides until a translucent layer was formed; the samples were kept moist at all times, air dried to a wet condition. X-ray data were collected in a Siemens D5000 diffractometer, using CuKα radiation, scanning at 0.5°2θ/min from 2 to 40°2θ and 60 to 65°2θ; the relative humidity was not controlled during the data collection but runs were duplicated on freshly prepared wet samples. The resulting diffraction patterns in some cases contained very minor peaks of fine ash components, volcanic glass, fine-grained plagioclase, K-feldspar and cristobalite. The corresponding diffraction pattern of the fine ash separated from the <2 μm material was subtracted from those of the samples, by using the diffraction software, to improve the data for the clay minerals. The subtraction was limited to reduce the background and the broad 6–14°2θ diffraction peak of glass without essentially affecting the intensity of the 00*l* clay peaks. Experimental patterns of the interstratified minerals were compared with those calculated using NEWMOD (Reynolds and Reynolds, 1996). Simulated patterns were mixed in various proportions to create composites similar to the experimental patterns. However, strong differences between the intensities of the 00*l* reflections of smectite, kaolinite and smectite-kaolinite interstratifications did not allow precise estimation of their abundance and limited the use of the simulated patterns to the assessment of interplanar distances, peak shapes and approximate mineral content. These, plus the relative intensities of the characteristic 00*l* peaks, allowed us to estimate abundances by differentiating between the most and least abundant clay components.

Smectite and vermiculite were differentiated by saturation with Mg and glycerol. Kaolinite was identified by its 001, 002 and 003 reflections that were not shifted by glycol, and by the absence of the 14 Å chlorite peak. Smectite was recognized as $1H_2O$- and $2H_2O$-smectite; glycolation was used to differentiate smectite, chlorite, kaolinite and the interstratified minerals. Broad diffraction bands extending from 6–14°2θ and 20–30°2θ characterized volcanic glass. The occurrence of cristobalite was confirmed when its 101 peak at 4.04 Å, which coincides with the 201 peak of plagioclase, was more intense than the 040 peak at 3.20–3.21 Å of plagioclase and K-feldspar.

Morphology and chemical composition were studied by scanning electron microscopy (SEM) coupled with energy dispersive X-ray fluorescence spectrometry (EDXRF) on fractured surfaces and on <2 μm and <0.5 μm fractions freeze dried and sputtered with graphite. The EDXRF was calibrated with orthoclase, phlogopite, albite and kaolinite reference samples; no additional provisions were taken to separate possible contaminants. Structural formulae were calculated respectively for the $O_{10}(OH)_2$ half-cell of montmorillon-

ite, the $(OH)_6$ cell of hydroxyl complexes (Güven, 1988; Moore and Reynolds, 1997; Bailey, 1988a,b), and the hypothetical $Si_4Al_{2.5}O_{10}(OH)_{3.5}$ for smectite (0.75)-kaolinite mixed layers. Iron in smectite was calculated as Fe^{3+}, based on the dioctahedral character of smectite as shown by chemical composition and the position of the 060 reflection.

The rheology studies were performed on the <0.5 μm fraction suspended in demineralized water, free of chemical additives, at uniform solid/water ratios to assure minimal effects of water entrapment among the clay particles, and repeatedly centrifuged to eliminate the non-clay components. Of the two suspensions selected, one, from 26 m depth (Charcos), having smectite, kaolinite, and interstratified kaolinite-smectite, was dispersed as 15.45 wt.% solids in water; the second suspension, from 60 m depth, containing more smectite and less kaolinite, was dispersed at 14.02 wt.% solids in water. Measurements were performed in a Bohlin Controlled Stress Rheometer (Bohlin Instruments Ltd., England) using a stationary cup and rotating cylinder assembly, at a constant temperature of 25ºC, vibrating frequencies of 1 to 10 Hz. The measurements included yield stress tests to evaluate flow behavior and oscillatory tests to assess the shear dynamic response by varying the stress linearly with time while vibrated at distinct frequencies.

RESULTS

Upper strata of gravel and sand characterize the sedimentary sequence in the northern area of the Basin (Charcos), where clay is the minor component, intimately associated with fine ash. This ash contains volcanic glass, plagioclase, K-feldspar, cristobalite, quartz and minor clay (Figure 2). Its diffraction pattern

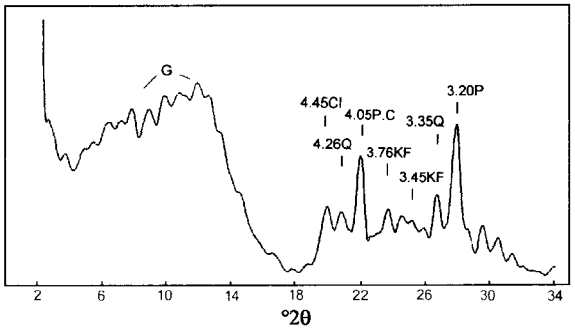

Figure 2. XRD pattern of the <2 μm fraction (Charcos) of fine ash, showing glass (G), plagioclase (P), K-feldspar (KF), quartz (Q), cristobalite (C) and clay minerals (Cl).

(Figure 2) was subtracted from those of the samples when needed to improve the resolution on the clay minerals.

The clay minerals occurring in the Basin (Table 1) are $1H_2O$- and $2H_2O$-smectite, kaolinite, interstratified R1-$1H_2O$-smectite (0.75)-kaolinite, R1-$2H_2O$-smectite (0.75)-kaolinite, R3-$2H_2O$-smectite (0.75)-kaolinite, R3-kaolinite (0.75)-$2H_2O$-smectite and R3-kaolinite (0.80)-$2H_2O$-smectite. The smectite-kaolinite mixed layers were recognized from patterns simulated with NEWMOD (Reynolds and Reynolds, 1996); their characteristic spacings are indicated in Table 2. The relative abundance of the minerals (Table 1) was estimated from the intensity of the 00*l* peaks in experimental patterns and in simulated patterns of clay composites. Among the mixed-layer minerals, R1-$2H_2O$-smectite (0.75)-kaolinite shows distinctive peaks at 24.51 and 10.96 Å; additional reflections at 7.29 and 3.67 Å may overlap those of R3-kaolinite (0.75)-$2H_2O$-smectite. Reichweite R3 interstratifications are well defined by peaks >27.12 Å. When there is 25% kaolin-

Table 1. Clay minerals of the Mexican Basin.

Depth (m)	1H-Sm[1]	2H-Sm	K	R1-K(0.25)-2H-Sm	R3-K(0.25)-2H-Sm	R3-K(0.75)-2H-Sm	R1-K(0.25)-1H-Sm
8		XX	XX	X	X	X	
10	X	XX	XX		X		
16	XXX		X		X		X
18	XX		XX		X		X
26		XXX	XX		X	X	
86		XXX	X		X		
90	X	XXX	X		X		
148		XXX				X	
218		X					
254		XXX				X	
262		XXX				X	
324	XXX	XXX					

[1] 1H-Sm, $1H_2O$-smectite; 2H-Sm, $2H_2O$-smectite; K, kaolinite; R1-K(0.25)-2H-Sm, R1-$2H_2O$-smectite(0.75)-kaolinite; R3-K(0.25)-2H-Sm, R3-$2H_2O$-smectite(0.75)-kaolinite; R3-K(0.75)-2H-Sm, R3-kaolinite(0.75)-$2H_2O$-smectite; R1-K(0.25)-1H-Sm, R1-$1H_2O$-smectite(0.75)-kaolinite. The relative abundance of minerals is indicated by XXX when most abundant and X when least abundant, as estimated from the intensities of the 00*l* peaks in the experimental and in the simulated diffraction patterns. Analyses by XRD of the <0.5 μm fraction. Analyses of the <2.0 μm fraction indicated glass, plagioclase, K-feldspar, cristobalite and quartz in most samples.

https://doi.org/10.1346/000986002762090344 Published online by Cambridge University Press

Table 2. Characteristic spacings (Å) of interstratified smectite-kaolinite recognized in the Mexican Basin.

Measured[1]										
R1 $1H_2O$-smectite(0.75)-kaolinite						11.23				3.14
R1 $2H_2O$-smectite(0.75)-kaolinite	24.51				10.96	7.29	3.67			
R3 $2H_2O$-smectite(0.75)-kaolinite		27.12		17.44	13.37	10.73				3.08
R3 kaolinite(0.75)-$2H_2O$-smectite	35.65		18.96		12.25		9.68	7.48	3.67	3.26
R3 kaolinite(0.80)-$2H_2O$-smectite	41.03		20.05		13.12		9.79	7.25	3.67	3.28
Calculated[2]										
R1 $1H_2O$-smectite(0.75)-kaolinite						11.47				3.16
R1 $2H_2O$-smectite(0.75)-kaolinite		25.73				11.15		7.34	3.63	
R3 $2H_2O$-smectite(0.75)-kaolinite		26.27		17.48	13.18	10.49				3.07
R3 kaolinite(0.75)-$2H_2O$-smectite	35.31		18.39		12.20	9.20	7.32	3.64	3.30	
R1 kaolinite(0.75)-Gly-smectite			28.66						7.78	3.47
R3 kaolinite(0.80)-Gly-smectite				19.88	13.12				7.66	3.48

[1] Spacings measured experimentally
[2] Spacings calculated using NEWMOD (Reynolds and Reynolds, 1996); calculation parameters are kaolinite, $1H_2O$- and $2H_2O$-smectite dioctahedral 0.3Fe, CuKα.

ite, the peaks at 17.44, 13.37 and 3.08 Å are resolved from those of smectite; when there is 75–80%, larger spacings occur at 18.96–20.05, 12.25, 9.68–9.79, 7.48–7.25, 3.67 and 3.26–3.28 Å. R1-$1H_2O$-smectite (0.75)-kaolinite has reflections at 11.23 and 3.14 Å near the ~11 Å peak of R1-$2H_2O$-smectite (0.75)-kaolinite and the 3.10 Å peak of smectite.

$2H_2O$-smectite, kaolinite, interstratified R1-$2H_2O$-smectite (0.75)-kaolinite, R3-$2H_2O$-smectite (0.75)-kaolinite and R3-kaolinite (0.75)/$2H_2O$-smectite occur at 8–10 m depth (Table 1, Figure 3A,B) and 26–90 m (Figure 4A,B,C). The $2H_2O$-smectite is more abundant than kaolinite or the mixed-layer minerals; adsorption of ethylene glycol permitted differentiation of kaolinite from smectite and interstratified minerals. At 16–18 m (Figure 3C,D), $1H_2O$-smectite predominates over kaolinite, R3-$2H_2O$-smectite (0.75)-kaolinite and R1-$1H_2O$-smectite (0.75)-kaolinite. At 26 and at 86 m $2H_2O$-smectite is more common than kaolinite and interstratified R3-$2H_2O$-smectite (0.75)-kaolinite, which tend to decrease (Figure 4A,B). At 90 m, kaolinite and interstratified kaolinite-smectite are less significant (Figure 4C), and at 148 m they are practically non-existent (Figure 4D). From 148 m and down to 324 m, $2H_2O$-smectite is essentially the single clay component (Figure 4E). The minerals are dioctahedral, d_{060} 1.496–1.50 Å, but occasional weak reflections at 1.52 Å were recorded.

The mineralogical sequence is reversed in the southern area of the Basin (Tezonco) where 46 m, from 14 to 60 m, of mudstones containing essentially $2H_2O$-smectite rest upon thick (60–286 m) strata of ash containing minor smectite, kaolinite and interstratified smectite-kaolinite.

The morphology of the <2 μm fraction is characterized, at 10 m, by volcanic glass, glass transforming to pseudohexagonal platelets and high-Si spherical particles presumably of opal (Figure 5A). At 86 m, diatoms, glass shards, plagioclase, glass transforming to hexago-

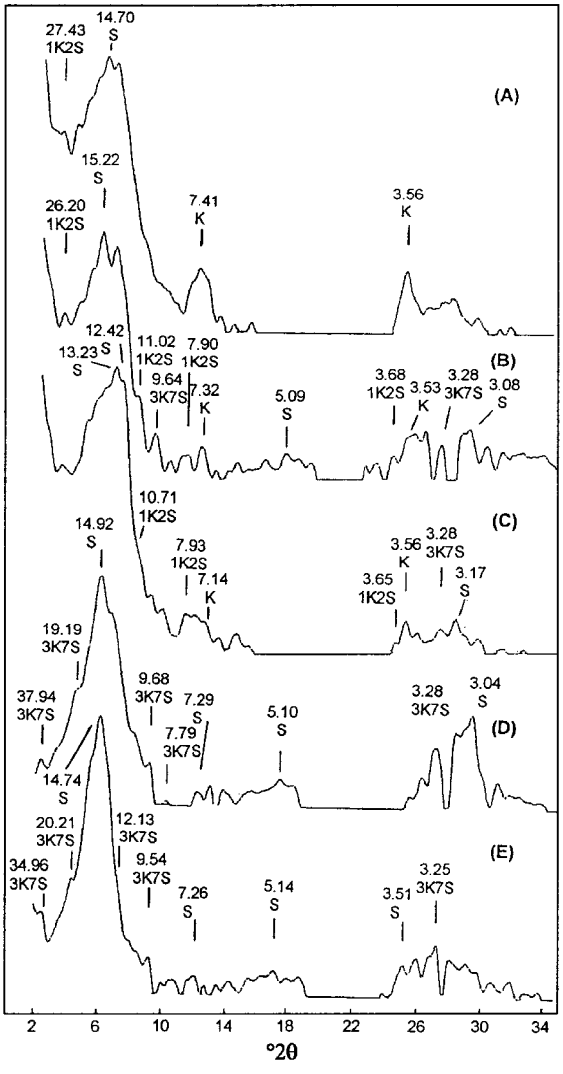

Figure 3. XRD patterns of the <0.5 μm fraction (Charcos): (A) 8 m deep; (B) 10 m; (C) 16 m; (D) 18 m. S: $1H_2O$- or $2H_2O$-smectite; K: kaolinite; 1K2S: R1 $2H_2O$-smectite (0.75)-kaolinite; 3K7S: R3 kaolinite (0.75)-$2H_2O$-smectite.

https://doi.org/10.1346/000986002762090344 Published online by Cambridge University Press

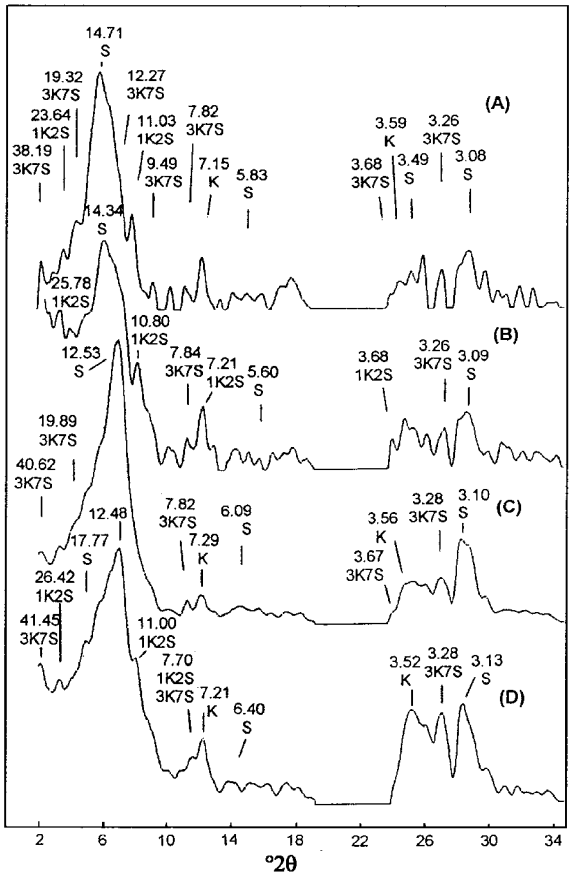

Figure 4. XRD patterns of the <0.5 μm fraction (Charcos): (A) 26 m deep; (B) 86 m; (C) 90 m; (D) 148 m; (E) 254 m. S: $1H_2O$- or $2H_2O$-smectite; K: kaolinite; 1K2S: R1 $2H_2O$-smectite (0.75)-kaolinite; 3K7S: R3 kaolinite (0.75)-$2H_2O$-smectite.

nal platelets and hexagonal platelets of smectite are recognized (Figure 5B,C) and, at 92 m, are smectite platelets, plagioclase and glass (Figure 5D). At 188 m, glass partially transformed to smectite is present (Figure 5E), and, at 254 m, smectite lamellae occur with glass partially altered to hexagonal platelets (Figure 5F).

Analysis by EDXRF analyses of single fragments and crystals selected by SEM indicate the occurrence of glass (Table 3), pseudohexagonal platelets of partially transformed glass (Table 4), glass almost totally transformed to smectite (Table 5), smectite lamellae (Table 6), interstratified smectite-kaolinite (Tables 7 and 8) and hydroxyl complexes (Table 9). The data do not indicate a particular correlation with depth, although some minerals are more common than others at certain depths.

DISCUSSION

The principal clay minerals in the upper strata of gravel and sand (Table 1, Figures 3 and 4) are $1H_2O$-smectite and $2H_2O$-smectite, together with minor kaolinite and interstratified smectite-kaolinite mixed layers that do not occur in the lower mudstones. Kaolinite could form from K-feldspar in the acid environment of high hydraulic conductivity and permeability prevailing in the gravel. Smectite was transformed from volcanic glass. The recognition of $1H_2O$- and $2H_2O$-smectite could be related to the lack of humidity control during the XRD collection of data. However, the persistence of the two smectite types in repeated analyses suggests a possible dependence on the adsorbed cations, layer-charge distribution or interstratifications of distinct smectite layers (Newman and Brown, 1987; Newman, 1987; Moore and Reynolds, 1997).

Glass predominates in the gravel (Figure 5, Table 3). It is high in SiO_2 (Table 3), between 92.17 and 81.89 wt.%, average 85.24 wt.% SiO_2, 0.54 TiO_2, 8.10 Al_2O_3, 2.86 Fe_2O_3, 0.19 MnO, 1.20 MgO, 0.71 CaO, 0.46 Na_2O and 0.69 K_2O. One fragment (sample Ch81, Table 3) contains 92.17 wt.% SiO_2, close to chalcedony or opal. There are some high-Si particles possibly of opal; however, the diffraction data did not confirm the occurrence of quartz or cristobalite in the <0.5 μm fractions. The ratios of SiO_2 to the remaining components of glass are higher than those recognized for the other associated minerals (Figure 6).

Table 3. Chemical composition (wt.%) of glass.

Sample[1]	Ch6	Ch12	Ch15	Ch17	Ch20	Ch81	Ch24	Ch25	Ch27	T2	T2	T4	Average
Depth (m)	10	10	10	10	10	10	10	10	10	60	63	77	
SiO_2	88.11	88.40	81.89	84.10	88.54	92.17	83.57	84.17	81.97	83.72	82.19	84.15	85.24
TiO_2	0.55	0.16	1.08	0.54	0.45	0.58	0.95	0.33	0.83	0.36	0.63	0	0.54
Al_2O_3	6.35	6.96	11.56	9.69	6.99	3.90	7.37	8.10	9.84	8.41	9.98	8.03	8.10
Fe_2O_3	1.13	1.87	3.16	2.70	1.32	2.28	4.49	4.29	3.74	3.07	2.18	4.06	2.86
MnO	0.01	0.23	0	0.31	0	0.06	0.51	0.38	0.12	0.34	0.23	0.11	0.19
MgO	0.61	0.94	0.89	0.85	0.59	0.37	1.22	1.73	1.67	1.61	2.38	1.53	1.20
CaO	0.80	0.56	0.22	0.80	0.55	0.12	1.29	0.57	0.48	0.88	0.82	1.48	0.71
Na_2O	0.74	0.64	0.45	0.50	0.61	0.52	0.11	0.17	0.80	0.60	0.43	0	0.46
K_2O	1.70	0.24	0.76	0.51	0.96	0	0.50	0.27	0.55	1.02	1.17	0.64	0.69
Total	100.00	100.00	100.00	100.00	100.00	100.00	100.00	100.00	100.00	100.00	100.00	100.00	100.00

[1] Analyses by EDXRF on fragments selected by SEM

https://doi.org/10.1346/000986002762090344 Published online by Cambridge University Press

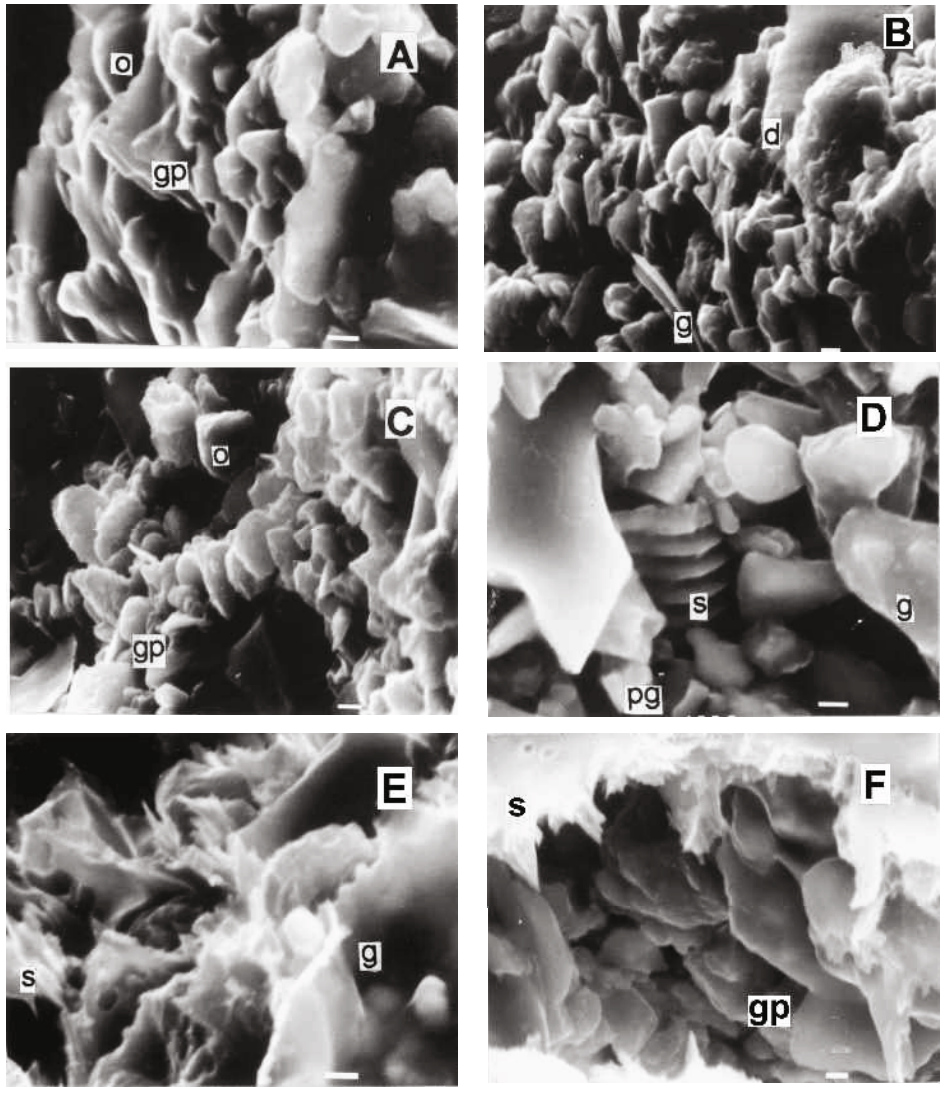

Figure 5. SEM images of the <2 μm fraction (Charcos) showing: (A) 10 m deep, glass transforming to hexagonal platelets (gp), opal (o); (B) 86 m, diatom (d), glass (g), plagioclase (pg), glass transforming to hexagonal platelets (gp); (C) 86 m, smectite platelets (s), glass (g); (D) 92 m, smectite platelets (s), glass (g), plagioclase (pg); (E) 188 m, glass (g), smectite (s); (F) 254 m, smectite (s), glass transforming to hexagonal platelets (gp). The horizontal bar represents 1 μm

Glass transforms to hexagonal platelets (Figure 5A,B,C,D,F). Their composition, calculated to the $O_{10}(OH)_2$ montmorillonite half-cell, allows differentiation between partially formed platelets, or in the process of transformation from glass, with excess Si^{4+} of 4.55–4.10 a.p.f.u. (atoms per formula unit) (Table 4) and those platelets of Si^{4+} between 4.08 and 4.03 a.p.f.u. (Table 5) almost fully transformed to smectite. Both platelets (Tables 4 and 5) have ratios of SiO_2 to other components lower than those of glass (Table 3) that conform to a linear correlation of decreasing SiO_2 and increasing octahedral components (Figure 6). There are platelets high in Al_2O_3 (samples Ch18, Ch40, in Table 4; T57, in Table 5), Fe_2O_3 (T72, in Table 5) and MgO (Ch51, in Table 4).

Platelets with $4.55 > Si^{4+} > 4.10$ a.p.f.u., which are predominant in the upper gravel, show, as expected, an inverse correspondence between ^{IV}Si and $^{VI}Al+Ti+Fe^{3+}+Mn+Mg$ (Figure 7A) that ends with the highest occupancy of octahedral 2.0 a.p.f.u. per 4.0 a.p.f.u. tetrahedra. The established linear correlation (Figure 7A) sustains the desilicification of glass towards smectite. Octahedral Mg+Mn (Figure 7B) is approximately uniform between 0.38 and 0.10 a.p.f.u. for large variations of $^{VI}Al+Fe^{3+}+Ti$ between 0.98 and 1.65 a.p.f.u.; two samples high in Mg (Ch41 and Ch51, Table 4) fall outside this range. The interlayer charge, between 0.38 and 0.13, is independent of the composition of the octahedral sheet (Table 4, Figure 7C). Platelets with $4.08 > Si^{4+} > 4.03$ a.p.f.u. (Table 5)

https://doi.org/10.1346/000986002762090344 Published online by Cambridge University Press

Table 4. Chemical composition (wt.%) of partially transformed glass.

Sample[1]	T62	T59	T52	Ch22	Ch41	Ch19	Ch9	Ch23	Ch37	Ch50
Depth (m)	2	2	2	10	10	10	10	10	10	18
SiO_2	78.27	78.10	77.71	77.45	77.09	75.57	73.16	73.03	73.45	71.67
TiO_2	0.15	0.11	0.27	0.45	0.29	0.21	0.43	0.61	0.82	0.73
Al_2O_3	12.03	12.18	12.22	13.74	13.86	15.34	15.70	15.57	17.46	12.70
Fe_2O_3	3.52	3.34	4.34	3.85	2.41	4.98	2.81	7.13	2.87	9.91
MnO	0	0.04	0.13	0.73	0	0.07	0.15	0.09	0.12	0.50
MgO	2.70	3.11	2.83	1.54	5.14	2.30	1.18	1.15	1.49	3.00
CaO	1.56	1.12	0.68	0.66	0.30	1.00	0.45	0.92	1.01	1.23
Na_2O	0.56	1.05	0.76	0.70	0.77	0.52	0.94	0.45	0.76	0.25
K_2O	1.21	0.95	1.08	0.88	0.15	0.98	5.18	1.05	2.02	0.79
Total	100.00	100.00	100.00	100.00	100.00	100.00	100.00	100.00	100.00	100.00
Si^{4+}	4.55	4.54	4.53	4.51	4.45	4.38	4.36	4.31	4.31	4.26
$^{VI}Al^{3+}$	0.83	0.83	0.84	0.94	0.94	1.05	1.10	1.08	1.21	0.89
Ti^{4+}	0.01	0	0.01	0.02	0.01	0.01	0.02	0.03	0.04	0.03
Fe^{3+}	0.15	0.15	0.19	0.17	0.10	0.22	0.13	0.32	0.13	0.44
Mn^{2+}	0	0	0.01	0.04	0	0	0.01	0	0.01	0.03
Mg^{2+}	0.23	0.27	0.25	0.13	0.44	0.20	0.10	0.10	0.13	0.27
Σ oct	1.22	1.26	1.29	1.30	1.50	1.48	1.36	1.53	1.50	1.66
Ca^{2+}	0.10	0.07	0.04	0.04	0.02	0.06	0.03	0.06	0.06	0.08
Na^{+}	0.06	0.12	0.09	0.08	0.09	0.06	0.11	0.05	0.09	0.03
K^{+}	0.09	0.07	0.08	0.07	0.01	0.07	0.39	0.08	0.15	0.06
Σinterlayer charge	0.35	0.33	0.25	0.23	0.13	0.26	0.56	0.25	0.36	0.25

Sample	Ch51	Ch82	Ch42	Ch18	Ch16	Ch40	T56	T54	Average
Depth (m)	218	92	218	10	10	10	2	2	
SiO_2	71.75	71.42	71.86	71.13	69.41	70.78	69.02	68.52	73.20
TiO_2	0.41	0.92	0.35	0.12	0.84	0.77	0.16	3.27	0.60
Al_2O_3	8.71	17.49	17.61	20.47	17.40	19.97	16.99	15.29	15.24
Fe_2O_3	3.50	6.71	4.28	4.85	7.87	2.32	6.30	6.80	4.67
MnO	0.33	0.11	0	0.16	0	0.03	0	0.03	0.14
MgO	13.88	1.62	1.13	1.12	1.54	3.73	4.24	2.72	3.02
CaO	0.68	0.94	3.06	0.75	0.99	0.88	1.36	1.57	1.06
Na_2O	0.74	0.77	1.71	0.65	0.75	1.06	0.41	1.01	0.77
K_2O	1.18	0.54	2.66	0.75	1.19	0.47	1.51	0.78	1.29
Total	100.00	100.00	100.00	100.00	100.00	100.00	100.00	100.00	100.00
Si^{4+}	4.23	4.19	4.19	4.17	4.14	4.13	4.11	4.10	4.31
$^{VI}Al^{3+}$	0.61	1.21	1.21	1.41	1.22	1.37	1.19	1.08	1.06
Ti^{4+}	0.02	0.04	0.02	0.01	0.04	0.03	0.01	0.15	0.03
Fe^{3+}	0.16	0.30	0.19	0.21	0.35	0.10	0.28	0.31	0.21
Mn^{2+}	0.02	0.01	0	0.01	0	0	0	0	0.01
Mg^{2+}	1.22	0.14	0.10	0.10	0.14	0.32	0.38	0.24	0.26
Σ oct	2.01	1.70	1.51	1.74	1.75	1.84	1.86	1.78	1.56
Ca^{2+}	0.04	0.06	0.19	0.05	0.06	0.05	0.09	0.10	0.07
Na^{+}	0.08	0.09	0.19	0.07	0.09	0.12	0.05	0.12	0.09
K^{+}	0.09	0.04	0.20	0.06	0.09	0.03	0.11	0.06	0.10
Σinterlayer charge	0.26	0.25	0.77	0.22	0.30	0.26	0.34	0.38	0.32

[1] Analyses by EDXRF on platelets selected by SEM

show an essentially constant correlation between the tetrahedral and octahedral sheets (Figure 7), with insufficient octahedral occupancy. In the octahedral sheet there is a distinct inverse relation between Mg+Mn and $^{VI}Al+Fe^{3+}+Ti$ (Figure 7B), similar to that shown by smectite when decreasing the latter ions while increasing the former. The straight line shown in Figure 7B marks the limit below which smectite platelets and lamellae (Table 6) and hexagonal platelets (Table 5) keep the composition of their octahedral sheets. The interlayer charge of these platelets (Figure 7C) increases as the occupancy of the octahedral sheet decreases, as in smectite.

In the lower mudstones, smectite lamellae are formed directly from glass (Figure 5E,F). The compositions shown (Table 6) indicate low ratios of SiO_2 to the octahedral components (Figure 6) that maintain linear correlation with those of glass and the hexagonal platelets. The tetrahedral sheet shows replacement and there is low occupancy of the octahedral sheet

https://doi.org/10.1346/000986002762090344 Published online by Cambridge University Press

Table 5. Chemical composition (wt.%) of glass transformed to smectite.

Sample[1]	T65	T10	T66	T57	T67	T74	T72	T75	T73	T55	Average
Depth (m)	3	35	3	2	3	218	218	218	218	2	
SiO_2	69.04	68.54	68.22	69.51	67.88	68.00	66.20	66.99	65.57	67.64	68.04
TiO_2	0.35	1.24	0.43	0.35	0.96	0.70	1.13	0.18	0.82	0.87	0.80
Al_2O_3	17.95	15.22	17.48	22.93	16.76	17.92	13.91	16.98	13.52	18.00	17.12
Fe_2O_3	3.41	2.96	4.13	3.64	5.99	5.28	13.84	6.35	9.69	6.37	6.11
MnO	0.25	0.15	0.23	0.18	0	0.23	0.04	0.09	0.09	0.13	0.12
MgO	5.80	8.36	5.85	1.63	4.44	4.04	1.92	5.01	4.08	4.43	4.31
CaO	1.19	1.33	1.25	1.28	2.21	1.31	1.85	1.08	1.46	1.01	1.36
Na_2O	1.34	0.97	1.39	0	0.90	0.36	0.23	0.36	1.96	0.37	0.79
K_2O	0.68	1.25	1.02	0.48	0.86	2.16	0.87	2.96	2.81	1.19	1.35
Total	100.00	100.00	100.00	100.00	100.00	100.00	100.00	100.00	100.00	100.00	100.00
Si^{4+}	4.08	4.08	4.06	4.06	4.06	4.06	4.05	4.04	4.04	4.03	4.07
$^{VI}Al^{3+}$	1.25	1.07	1.23	1.58	1.18	1.26	1.00	1.21	0.98	1.26	1.21
Ti^{4+}	0.02	0.06	0.02	0.02	0.04	0.03	0.05	0.01	0.04	0.04	0.04
Fe^{3+}	0.15	0.13	0.18	0.16	0.27	0.24	0.64	0.29	0.45	0.29	0.27
Mn^{2+}	0.01	0.01	0.01	0.01	0	0.01	0	0	0	0.01	0.01
Mg^{2+}	0.51	0.74	0.52	0.14	0.40	0.36	0.18	0.45	0.37	0.39	0.38
Σ oct	1.94	2.00	1.96	1.90	1.89	1.90	1.87	1.96	1.85	1.99	1.91
Ca^{2+}	0.08	0.08	0.08	0.08	0.14	0.08	0.12	0.07	0.10	0.06	0.09
Na^{+}	0.15	0.11	0.16	0	0.10	0.04	0.03	0.04	0.23	0.04	0.09
K^{+}	0.05	0.09	0.08	0.04	0.07	0.16	0.07	0.23	0.22	0.09	0.10
Σinterlayer charge	0.35	0.38	0.40	0.20	0.45	0.37	0.34	0.41	0.65	0.26	0.37

[1] Analyses by EDXRF on platelets selected by SEM

(Figure 7A). Among the octahedral ions, $^{VI}Al+Fe^{3+}+Ti$ decrease as Mg+Mn increase; the correlation is linear, different from that of the high Si^{4+} platelets but similar to that of the low Si^{4+} ones (Figure 7B). The interlayer charge increases with decreasing occupancy of the octahedral sheet (Figure 7C); the highest charges are associated with tetrahedral replacement by $^{IV}Al^{3+}$ in addition to low occupancy of the octahedral sheet (samples Ch29, Ch47 and Ch28, in Table 6, Figure 7C,D).

Table 6. Chemical composition (wt.%) of smectite.

Sample[1]	Ch28	Ch43	Ch29	Ch47	T71	Ch7	T53	Ch32	Ch31	Ch48	Ch34	Average
Depth (m)	90	218	90	218	218	10	2	90	90	218	10	
SiO_2	55.99	59.25	62.30	62.19	65.49	64.96	65.73	66.36	66.81	66.24	67.27	65.26
TiO_2	3.33	1.83	0.25	0.31	0.95	1.21	0.54	0.76	0.61	1.09	1.34	0.78
Al_2O_3	19.34	18.95	24.63	23.59	20.80	17.37	17.68	20.33	21.30	17.93	19.07	20.30
Fe_2O_3	10.18	14.73	1.96	2.42	8.45	11.56	4.79	6.17	4.81	5.73	5.30	5.69
MnO	1.00	0.01	0.07	0.07	0	0.14	0.45	0.14	0	0.45	0.10	0.16
MgO	1.69	0.70	0.85	2.21	2.16	1.20	4.43	1.51	0.52	2.44	3.70	2.11
CaO	5.14	2.28	5.42	5.29	0.83	1.63	4.03	1.98	2.26	3.71	1.48	2.96
Na_2O	2.96	0.64	4.11	3.68	0.60	0.18	0.63	2.09	3.36	2.18	1.08	1.99
K_2O	0.37	1.62	0.41	0.25	0.70	1.77	1.72	0.67	0.34	0.24	0.66	0.75
Total	100.00	100.00	100.00	100.00	100.00	100.00	100.00	100.00	100.00	100.00	100.00	100.00
Si^{4+}	3.53	3.69	3.76	3.76	3.92	3.96	3.97	3.97	3.99	3.99	4.00	3.93
$^{IV}Al^{3+}$	0.47	0.31	0.24	0.24	0.08	0.04	0.03	0.03	0.01	0.01	0	0.07
$^{VI}Al^{3+}$	0.96	1.08	1.52	1.44	1.38	1.21	1.23	1.41	1.49	1.26	1.34	1.36
Ti^{4+}	0.16	0.09	0.01	0.01	0.04	0.06	0.02	0.03	0.03	0.05	0.06	0.04
Fe^{3+}	0.48	0.69	0.09	0.11	0.38	0.53	0.22	0.28	0.22	0.26	0.24	0.26
Mn^{2+}	0.05	0	0	0	0	0.01	0.02	0.01	0	0.02	0.01	0.01
Mg^{2+}	0.16	0.06	0.08	0.20	0.19	0.11	0.40	0.13	0.05	0.22	0.33	0.19
Σ oct	1.81	1.93	1.70	1.77	2.00	1.91	1.90	1.86	1.78	1.82	1.97	1.86
Ca^{2+}	0.35	0.15	0.35	0.34	0.05	0.11	0.26	0.13	0.14	0.24	0.09	0.19
Na^{+}	0.36	0.08	0.48	0.43	0.07	0.02	0.07	0.24	0.39	0.25	0.13	0.23
K^{+}	0.03	0.13	0.03	0.02	0.05	0.14	0.13	0.05	0.03	0.02	0.05	0.06
Σinterlayer charge	1.09	0.51	1.21	1.13	0.23	0.37	0.73	0.55	0.70	0.75	0.36	0.67

[1]Analyses by EDXRF on platelets selected by SEM

https://doi.org/10.1346/000986002762090344 Published online by Cambridge University Press

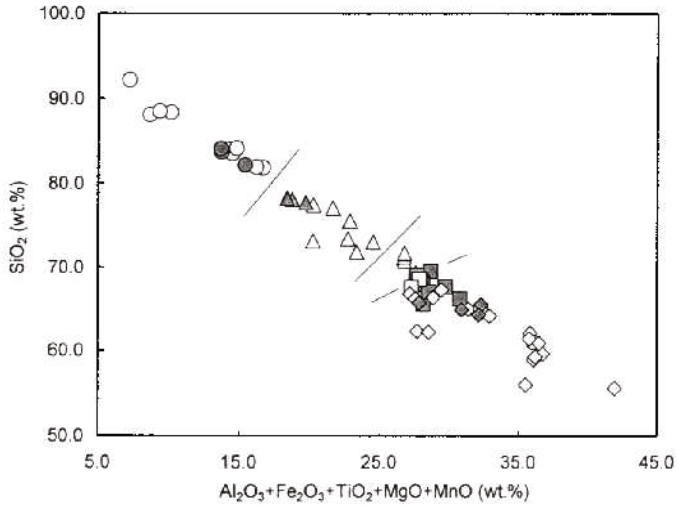

Figure 6. Correlation between the tetrahedral and octahedral components of glass (○), glass partially transformed to hexagonal platelets (△), smectite platelets (□), smectite lamellae and interstratified smectite-kaolinite (◇), from the northern (Charcos: open symbols) and southern (Tezonco: shaded symbols) areas. Straight lines mark the limits between the minerals.

The compositions shown for smectite (Table 6) correspond with montmorillonite. Some compositions (Ch28 and Ch43, in Table 6) have high contents of $^{IV}Al^{3+}$ that are in the range of beidellite. There are samples of high interlayer charge within the 0.2–0.60 equivalents common to montmorillonite, but others (samples Ch29, Ch47, Ch28, in Table 6) are near the 0.6–0.9 values accepted for vermiculite (Suquet *et al.*, 1975, 1977; Güven, 1988). At these high values there is not much difference in the swelling of the layers (Mering and Pedro, 1969; Suquet and Pezerat, 1987, 1988). The interlayer charge attains values >1.09 when $^{IV}Al^{3+}$ is $\geqslant$0.24 a.p.f.u. and the cation occupancy in the octahedral sheet is $\leqslant$1.81 a.p.f.u.; it tends to decrease as the occupancy of the octahedral sheet and Fe^{3+} increase (Figure 7C,D). The predominant $^{VI}Al^{3+}$ confirms the dioctahedral character of smectite.

There are lamellae (Table 7) of lower SiO_2, higher Al_2O_3, Fe_2O_3 and MgO, and lower CaO, Na_2O and K_2O than expected for smectite. They maintain the same

Table 7. Chemical composition (wt.%) of interstratified smectite-kaolinite mixed layers.

Sample[1]	Ch30	Ch39	Ch46	Ch79	Ch45	Ch27	Ch44	T76	Ch84	T64	Ch80	Average
Depth (m)	90	10	218	86	218	90	218	218	92	2	86	
SiO_2	55.55	59.61	60.89	58.91	61.41	62.06	61.01	64.27	64.14	64.90	65.11	61.62
TiO_2	2.35	2.24	1.00	2.51	0.98	0.82	2.00	0.90	0.74	0.13	0.56	1.29
Al_2O_3	22.85	23.53	23.25	15.42	24.71	24.30	17.44	20.66	17.07	19.46	20.12	20.80
Fe_2O_3	13.96	7.25	7.77	10.84	7.50	8.10	12.32	7.24	7.71	5.50	7.88	8.73
MnO	0.23	0.26	0.22	0.46	0	0.01	0.11	0	0.14	0.02	0.20	0.15
MgO	2.52	3.47	4.25	6.87	2.59	2.62	4.22	3.40	7.30	5.86	3.56	4.24
CaO	1.62	2.45	0.88	1.12	1.04	0.85	1.44	1.30	1.45	0.99	1.14	1.30
Na_2O	0.11	1.12	1.15	0.49	1.01	0.60	0.72	0.91	0.41	1.15	0.75	0.77
K_2O	0.82	0.06	0.60	3.38	0.75	0.63	0.75	1.32	1.05	1.99	0.68	1.09
Total	100.00	100.00	100.00	100.00	100.00	100.00	100.00	100.00	100.00	100.00	100.00	100.00
Si^{4+}	3.45	3.61	3.68	3.69	3.69	3.72	3.75	3.87	3.88	3.90	3.91	3.74
$^{IV}Al^{3+}$	0.55	0.39	0.32	0.31	0.31	0.28	0.25	0.13	0.12	0.10	0.09	0.26
$^{VI}Al^{3+}$	1.12	1.29	1.33	0.83	1.45	1.44	1.02	1.33	1.10	1.29	1.33	1.23
Ti^{4+}	0.11	0.10	0.05	0.12	0.04	0.04	0.09	0.04	0.03	0.01	0.03	0.06
Fe^{3+}	0.65	0.33	0.35	0.51	0.34	0.37	0.57	0.33	0.35	0.25	0.36	0.40
Mn^{2+}	0.01	0.01	0.01	0.02	0	0	0.01	0	0.01	0	0.01	0.01
Mg^{2+}	0.23	0.31	0.38	0.64	0.23	0.23	0.39	0.30	0.66	0.53	0.32	0.38
Σ oct	2.13	2.05	2.13	2.13	2.06	2.08	2.07	2.01	2.15	2.07	2.04	2.08
Ca^{2+}	0.11	0.16	0.06	0.08	0.07	0.05	0.10	0.08	0.09	0.06	0.07	0.08
Na^{+}	0.01	0.13	0.13	0.06	0.12	0.07	0.09	0.11	0.05	0.13	0.09	0.09
K^{+}	0.06	0	0.05	0.27	0.06	0.05	0.06	0.10	0.08	0.15	0.05	0.08
Σinterlayer charge	0.29	0.45	0.29	0.48	0.31	0.23	0.34	0.38	0.32	0.42	0.29	0.34

[1] Analyses by EDXRF on platelets selected by SEM

https://doi.org/10.1346/000986002762090344 Published online by Cambridge University Press

Table 8. Chemical composition (wt.%) and structural formulae of interstratified smectite(0.75)-kaolinite.

Sample[1]	Ch30	Ch39	Ch46	Ch79	Ch45	Ch27	Ch44	T76	Ch84	T64	Ch80
Depth (m)	90	10	218	86	218	90	218	218	92	2	86
SiO_2	55.55	59.61	60.89	58.91	61.41	62.06	61.01	64.27	64.14	64.90	65.11
TiO_2	2.35	2.24	1.00	2.51	0.98	0.82	2.00	0.90	0.74	0.13	0.56
Al_2O_3	22.85	23.53	23.25	15.42	24.71	24.30	17.44	20.66	17.07	19.46	20.12
Fe_2O_3	13.96	7.25	7.77	10.84	7.50	8.10	12.32	7.24	7.71	5.50	7.88
MnO	0.23	0.26	0.22	0.46	0.00	0.01	0.11	0.00	0.14	0.02	0.20
MgO	2.52	3.47	4.25	6.87	2.59	2.62	4.22	3.40	7.30	5.86	3.56
CaO	1.62	2.45	0.88	1.12	1.04	0.85	1.44	1.30	1.45	0.99	1.14
Na_2O	0.11	1.12	1.15	0.49	1.01	0.60	0.72	0.91	0.41	1.15	0.75
K_2O	0.82	0.06	0.60	3.38	0.75	0.63	0.75	1.32	1.05	1.99	0.68
Total	100.00	100.00	100.00	100.00	100.00	100.00	100.00	100.00	100.00	100.00	100.00
Si^{4+}	3.69	3.86	3.93	3.94	3.95	3.98	4.01	4.13	4.14	4.17	4.17
Al^{3+}	0.31	0.14	0.07	0.06	0.05	0.02	0.00	0.00	0.00	0.00	0.00
Al^{3+}	1.47	1.65	1.70	1.16	1.82	1.82	1.35	1.57	1.30	1.47	1.52
Ti^{4+}	0.12	0.11	0.05	0.13	0.05	0.04	0.10	0.04	0.04	0.01	0.03
Fe^{3+}	0.70	0.35	0.38	0.55	0.36	0.39	0.61	0.35	0.37	0.27	0.38
Mn^{2+}	0.01	0.01	0.01	0.03	0.00	0.00	0.01	0.00	0.01	0.00	0.01
Mg^{2+}	0.25	0.34	0.41	0.69	0.25	0.25	0.41	0.33	0.70	0.56	0.34
Σ oct	2.55	2.47	2.54	2.54	2.47	2.50	2.48	2.28	2.42	2.31	2.28
Ca^{2+}	0.11	0.17	0.06	0.08	0.07	0.06	0.10	0.09	0.10	0.07	0.08
Na^{+}	0.01	0.14	0.14	0.06	0.13	0.07	0.09	0.11	0.05	0.14	0.09
K^{+}	0.07	0.00	0.05	0.29	0.06	0.05	0.06	0.11	0.09	0.16	0.06
Σinterlayer charge	0.31	0.49	0.32	0.51	0.33	0.24	0.36	0.40	0.34	0.44	0.31

[1] Analyses by EDXRF on platelets selected by SEM

linear correlation between SiO_2 and the remaining components observed for the other associated minerals (Figure 6). Their structural formulae, calculated for the smectite $O_{10}(OH)_2$ half-cell, indicate ^{IV}Al replacement between 0.10 and 0.55 a.p.f.u. and octahedral occupancy between 2.01 and 2.15 a.p.f.u., in excess of 2.0 (Table 7, Figure 7A). The Mg+Mn to $^{VI}Al+Fe^{3+}+Ti$ correlation follows the same pattern as for smectite (Figure 7B) but for equal contents of $^{VI}Al+Fe^{3+}+Ti$ the values of Mg+Mn are higher than expected for smectite, or they fall above the straight line shown in Figure 7B. The interlayer charges (Figure 7C,D) average 0.34, roughly half of that shown by smectite. These lamellae correspond with the interstratified smectite-kaolinite of structural formula intermediate between those of smectite and kaolinite. Structural formulae calculated for a hypothetical interstratified R3-2H_2O-smectite (0.75)-kaolinite (Table 1) indicate (Table 8) tetrahedral replacement (samples Ch30, Ch39, Ch46, Ch79, Ch45 and Ch27 in Table 8), octahedral cations ~2.50 a.p.f.u. and interlayer charges lower than those of smectite. Some samples (T76m Ch84, T64 and Ch80 in Table 8) show excess Si^{4+} and lower occupancy of the octahedral sheet. Sample Ch30 may correspond with interstratifications of beidellite and kaolinite.

Hydroxyl complexes (Table 9) were recognized at 16 m depth, where an acid environment of high hydraulic conductivity and permeability prevailed.

The composition of the octahedral sheet allows differentiation between the various minerals while establishing their common origin. Preceding data (Figures 6 and 7) illustrate differences among the minerals. The ratios between Al^{3+}, Fe^{3+} and Mg^{2+} are essentially the same for glass, partially-transformed glass, platelets, smectite and interstratified smectite-kaolinite (Figure 8), clearly confirming their common origin.

Kaolinite occurs, possibly formed from K-feldspar, in the gravel strata where hydraulic conductivity and permeability were high and the environment was acid, rich in organic material, removing Si^{4+} from diatoms. In the same strata, volcanic glass was simultaneously transformed to hexagonal platelets of composition tending towards smectite by removing Si and proportionally enriching the octahedral cations. Mg+Mn were partially dissolved from the glass or enriched at a lesser

Table 9. Chemical composition (wt.%) of hydroxyl complexes.

Depth (m)	16	16
Sample	69	70
SiO_2	0	0
TiO_2	2.87	2.16
Al_2O_3	64.60	66.98
Fe_2O_3	10.00	15.91
MnO	1.62	0
MgO	7.15	5.31
CaO	6.69	2.91
Na_2O	5.10	2.72
K_2O	1.97	4.01
Total	100.00	100.00

Analyses by EDXRF on lamellae selected by SEM

https://doi.org/10.1346/000986002762090344 Published online by Cambridge University Press

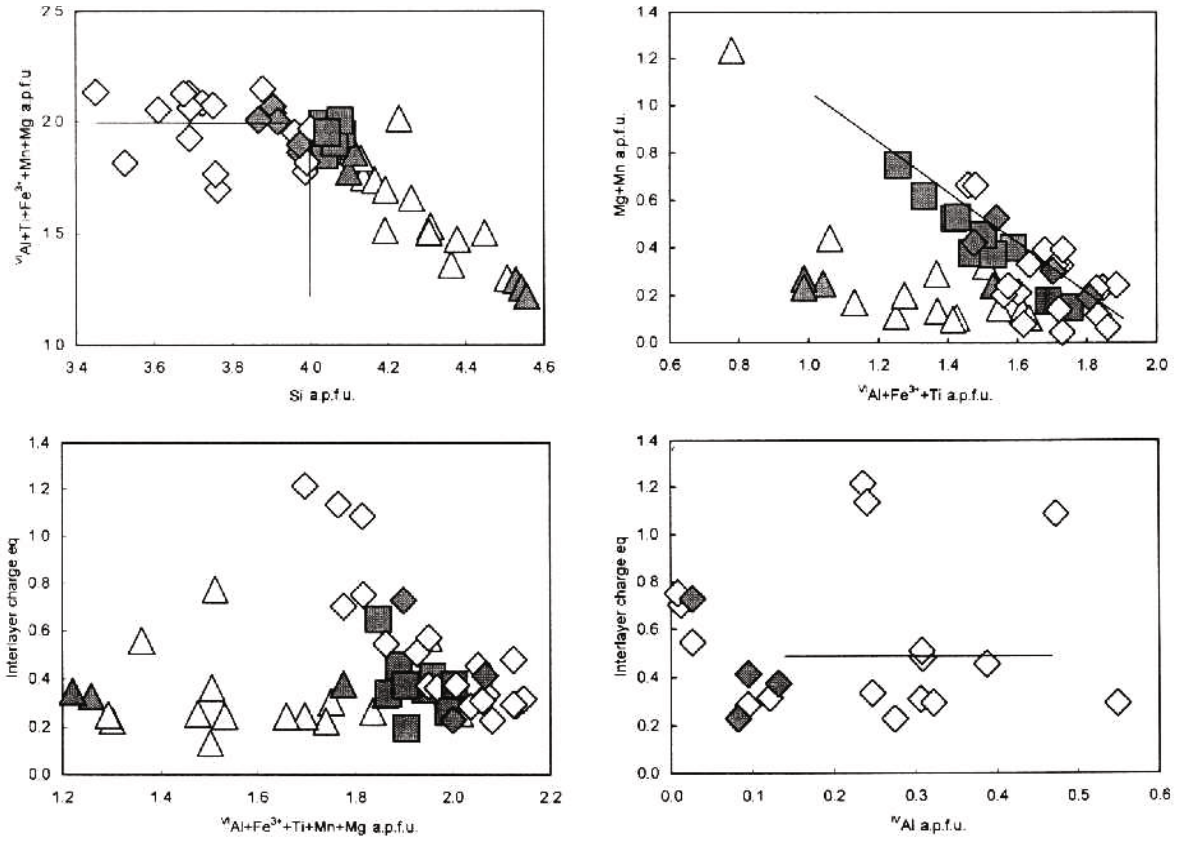

Figure 7. Compositional correlations between the tetrahedral and octahedral sheets of smectite: (A) (^{VI}Al+Ti+Fe+Mn+Mg) *vs.* (Si); (B) (Mg+Mn) *vs.* (^{VI}Al+Fe^{3+}+Ti); (C) (interlayer charge) *vs.* (^{VI}Al+ Fe^{3+}+Ti+Mn+Mg); (D) (interlayer charge) *vs.* (^{IV}Al). △: glass partially transformed to hexagonal platelets; □: smectite platelets; ◇: smectite lamellae and interstratified smectite-kaolinite, from the northern (Charcos: open symbols) and southern (Tezonco: shaded symbols) areas. Straight lines mark the limits between the minerals.

rate than Al+Fe+Ti. Interstratified smectite-kaolinite mixed layers, formed in these strata, sustain the transformation of kaolinite to smectite in a cation-enriched environment more favorable to the latter. At greater depths, in the mudstones, where hydraulic conductivity was much lower and flow was practically stagnant, glass was transformed directly to smectite lamellae. Conditions of drought and falling lake level favoring kaolinization (Hower *et al.*, 1976; April, 1981) could have developed. Smectite was formed (1) as hexagonal platelets, from volcanic glass and plagioclase in the high-permeability and hydraulic conductivity environment of the gravel and sand strata; (2) as irregular lamellae, from volcanic glass in the alkaline, low-permeability environment of the mudstones; and (3) from kaolinite via interstratified smectite-kaolinite.

The mineralogy of the clay fraction changes from $1H_2O$- and $2H_2O$-smectite, kaolinite and interstratified smectite-kaolinite in the gravel to predominant $2H_2O$-smectite in the mudstones; interlayer H_2O, cations and surface charge vary; smectite of distinct composition, high-Al, Fe or Mg, and beidellite occur. The transformation of glass to smectite progresses with depth and the morphology of smectite varies from platelets to lamellae. The chemical and physical environments, the chemical composition of minerals and fluids, the hydraulic conductivity and the permeability change. Thus it may be presumed that the physical behavior and stability of the sediments would be non-uniform across the Basin. The prevalence of dioctahedral smectite and

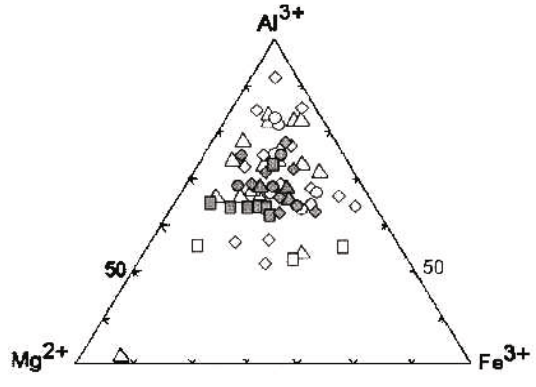

Figure 8. Correlation between the octahedral components of glass (○), glass transforming to platelets (△), smectite platelets (□), smectite lamellae and interstratified smectite-kaolinite (◇), from the northern (Charcos: open symbols) and southern (Tezonco: closed symbols) areas.

https://doi.org/10.1346/000986002762090344 Published online by Cambridge University Press

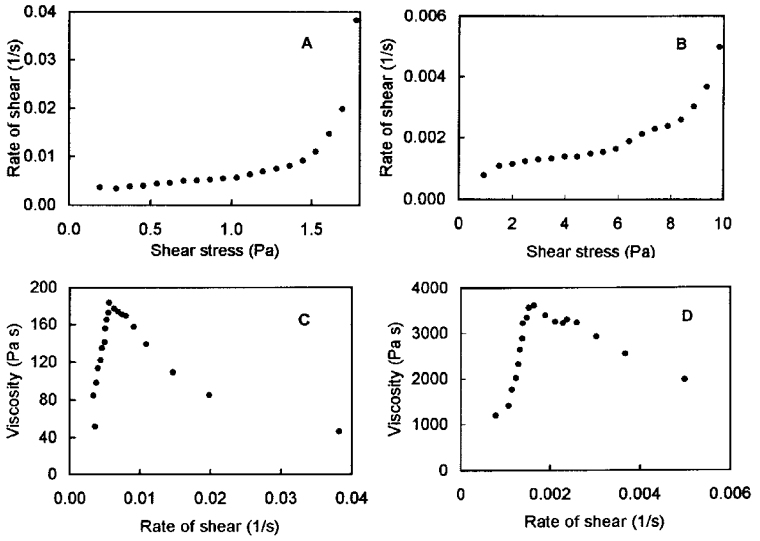

Figure 9. Flow curves of suspensions from the <2 μm clay fractions of sediments: (A,C) 26 m depth, 15.45 wt.% solids; (B,D) 60 m depth, 14.02 wt.% solids. They indicate non-Newtonian viscoelastic behavior, edge-to-edge or edge-to-face particle association at 26 m and high-energy face-to-face association at 60 m.

the absence of trioctahedral minerals and chlorite define by themselves a physically and chemically unstable system, opposed to the less expandable more mechanically stable trioctahedral smectite-chlorite systems known to occur in old sedimentary sequences (Jiang and Peacor, 1994; Chang *et al.*, 1986).

The physical behavior and stability of the clay fractions was assessed with rheological analyses. The rheological behavior of the clay particles depends on their interaction or on their structure and surface properties. The rheology of clay pastes, including montmorillonite, has been discussed by others (van Olphen, 1977; Brandenburg and Lagaly, 1988; Chen *et al.*, 1990; Heller and Keren, 2001). For the present purposes, two suspensions were selected for analysis, one, 26 m deep (Charco), having $1H_2O$- and $2H_2O$-smectite, kaolinite, and R3-$2H_2O$-smectite (0.75)-kaolinite, dispersed 15.45 wt.% solids in water, and the second, from 60 m depth, containing more $1H_2O$- and $2H_2O$-smectite, less kaolinite and R3-$2H_2O$-smectite (0.75)-kaolinite, dispersed 14.02 wt.% solids in water.

The flow curves (Figure 9A,B) show the variable shear rate/shear stress ratio and apparent viscosity (Figure 9C,D) that characterize non-Newtonian pseudoplastic behavior. The suspensions are thixotropic, reversible sol-gel transformations, with viscosity decreasing with shear but increasing upon rest. The suspension with the 26 m clay maintains a linear shear

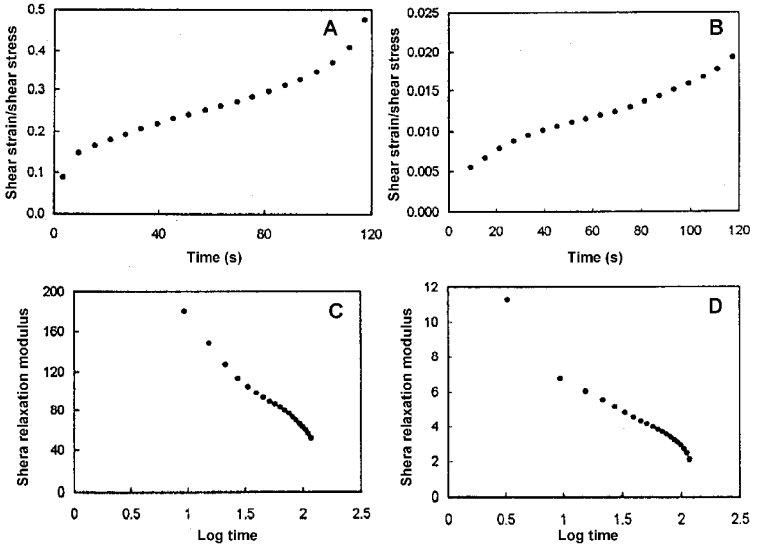

Figure 10. Shear strain/shear stress ratios and shear relaxation modulus of suspensions from the <2 μm clay fractions: (A,C) 26 m depth; (B,D), 60 m depth. The total elastic recoveries are 0.13 Pa^{-1} and 0.008 Pa^{-1}, respectively.

https://doi.org/10.1346/000986002762090344 Published online by Cambridge University Press

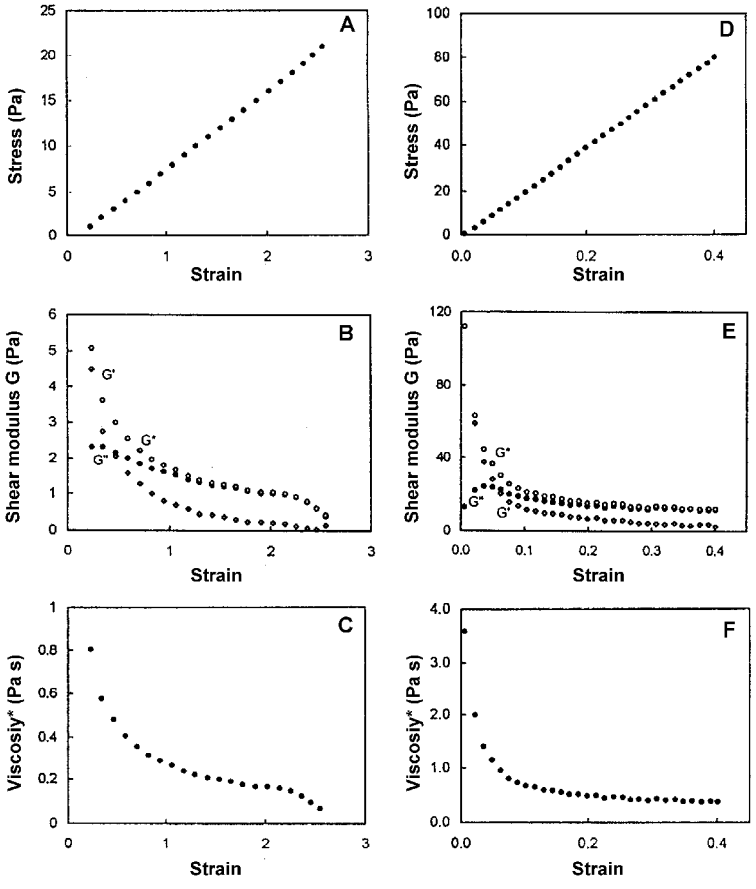

Figure 11. Shear dynamic response of the <2 μm clay fraction, from 60 m depth, when subjected to linear modulated shearing stress vibrating at frequencies of: (A,B,C) 1 Hz; (D,E,F) 5 Hz.

rate-shear stress correlation below 1.5 Pa and 0.01 s^{-1} (Figure 9A), whereas the apparent viscosity reaches a maximum 180 Pa s at 0.008 s^{-1} followed by a rapid descent (Figure 9C). The suspension of the 60 m clay has, at shear rates below 0.0025 s^{-1}, an approximately linear relation with the shear stress that includes two small broad bands attributed to two distinct forms of particle-particle association (Figure 9B). Its viscosity reaches a maximum of 3611 Pa s at a shear rate of 0.0016 s^{-1} and a second one of 3300 Pa s at 0.0024 s^{-1} shear, followed by a slow thinning descent (Figure 9D). The 26 m clay requires high shear rates to produce low shear and yield stresses and apparent viscosity, with low-energy edge-to-face or edge-to-edge particle interaction and thick water films between them. The 60 m clay develops, at low shear rates, high shear and yield stresses and viscosity, gels more and fluidizes less than the 26 m clay, in a face-to-face particle association of high energy and thin water films. The apparent viscosity decreases, when under viscous flow or at shear rates above the yield stress, at much faster pace in the 26 m clay (Figure 9C,D). Suspensions change from thickening to thinning, or from elastic to viscous behavior, respectively at shear stresses of 1.03 and 5.91 Pa. The shear strain/shear stress ratios (Figure 10A,B) are approximately linear within a short span of time; the total elastic recoveries are 0.15 Pa^{-1} and 0.008 Pa^{-1} respectively for the 26 m and 60 m clays. Creep compliance and the elastic part of the creep compliance ($J(t)-t/\eta$) show minimal deviation from zero. The stress relaxation modulus (G(t)), or reciprocal of the creep, are markedly distinct and conform to viscoelastic behavior (Figure 10C,D).

The 60 m clay suspension, under a stress increasing linearly with time while the frequency of vibration remained constant at 1 Hz, sufficiently small to assure linear viscoelastic behavior, developed stress <20 Pa (Figure 11A), shear modulus <5 Pa (Figure 11B) and kinematic viscosity <0.8 Pa s (Figure 11C). When the frequency of vibration was increased to 5 Hz the suspension required lower strain <0.4 to develop higher stress <80 Pa (Figure 11D), shear modulus <120 Pa (Figure 11E) and kinematic viscosity <4.0 Pa s (Figure 11F). At the low frequency of 1 Hz the shear storage dynamic modulus G' is higher than the shear dynamic loss modulus G'' (Figure 11B), or the energy is stored preferentially, whereas at the higher frequency of 5 Hz (Figure 11E), more energy is dissipated as heat than is stored. The dynamic response of the clay fraction changes with the frequency of the applied vibration; at

https://doi.org/10.1346/000986002762090344 Published online by Cambridge University Press

higher frequencies energy tends to be dissipated whereas at low frequencies it tends to be stored.

The rheological analyses of two clay fractions (1), 26 m deep, formed by $1H_2O$- and $2H_2O$-smectite, kaolinite and interstratified R3-$2H_2O$-smectite (0.75)-kaolinite, and (2), 60 m deep, containing $2H_2O$-smectite, slightly less $1H_2O$-smectite, kaolinite and R3-$2H_2O$-smectite (0.75)-kaolinite, have shown particle-particle interactions of different energy and behavior. Although both samples have the same minerals, small differences in their contents may also imply differences in surface charge, adsorbed water and cations, morphology and surface area that affect particle interaction, physical behavior and stability. The rheological data also indicate that clay fractions have a heterogeneous non-uniform behavior across the Basin. Depending on the distribution and content of clays in the sediments, or on the ratio of clay to non-clay components, differences in the behavior of the clays would modify to an extent the behavior of the bulk sediments.

CONCLUSIONS

Diagenesis of young sediments, in the Holocene-Pleistocene volcanogenic sequence of the Mexican Basin, was to smectite. In the gravel and sand strata, where fluids were rich in organics and permeability and hydraulic conductivity were high, smectite occurs in the forms of $1H_2O$- and $2H_2O$-smectite, associated with kaolinite, R3-$2H_2O$-smectite (0.75)-kaolinite and occasional R1-$2H_2O$-smectite (0.75)-kaolinite, R3-kaolinite (0.75)-$2H_2O$-smectite and R1-$1H_2O$-smectite (0.75)-kaolinite.

Smectite platelets were formed in the gravel strata from volcanic glass by gradual loss of Si^{4+} and proportional enrichment in Al^{3+}, Fe^{3+}, Ti^{4+}, Mg^{2+} and Mn^{2+}. When these platelets are still in the process of transformation, they have between 4.55 and 4.10 Si^{4+} a.p.f.u., and Mg+Mn and the interlayer charge remain approximately constant while $^{VI}Al+Fe^{3+}+Ti$ varies between 1.0 and 1.62 a.p.f.u. Further transformation reduces the Si^{4+} contents to 4.08–4.03 a.p.f.u., and Mg+Mn and the interlayer charge decrease proportionally with increasing $^{VI}Al+Fe^{3+}+Ti$, as in smectite. Interstratified smectite-kaolinite mixed layers are characterized by octahedral occupancies of 2.01–2.15 a.p.f.u., $^{IV}Al^{3+}$ 0.09–0.55 a.p.f.u. and interlayer charges about half of those of smectite. When the structural formulae are computed for a hypothetical cell $Si_4Al_{2.5-2.4}O_{10}(OH)_{3.5-3.2}$, corresponding to smectite (0.75–0.80)-kaolinite, octahedral occupancy is ~2.50 a.p.f.u., tetrahedral replacement is 0–0.31 a.p.f.u., and interlayer charges are 0.24–0.51 equivalents, some pointing to interstratifications of beidellite. The smectite-kaolinite interstratifications suggest the transformation of kaolinite to smectite in a high-cation environment is more favorable to the latter. Kaolinite is presumed to have formed from K-feldspar.

In the mudstones, where permeability and hydraulic conductivity were very low, and where high-cation alkaline fluids were practically stagnant, glass was transformed directly to $2H_2O$-smectite lamellae of ^{IV}Al between 0–0.47 a.p.f.u., octahedral occupancy 1.70–2.00 and interlayer charge 0.23–1.21 equivalents, some corresponding to beidellite. The interlayer charge increases with decreasing occupancy of the octahedral sheet and with tetrahedral replacement; the abundance of Mg+Mn is inverse to that of $^{VI}Al+Fe^{3+}+Ti$. Kaolinite and smectite-kaolinite interstratifications do not occur in the mudstones. The Si^{4+} removed from the glass is in the form of cristobalite almost through the complete sequence. Smectite was formed from glass and plagioclase to pseudohexagonal platelets and from kaolinite through smectite-kaolinite interstratifications in the high-hydraulic conductivity gravel strata, and from glass to irregular lamellae in the low-permeability mudstones. Volcanic glass, partially transformed glass, smectite platelets and lamellae, and interstratified smectite-kaolinite mixed layers have common Al^{3+}, Fe^{3+} and Mg^{2+} ratios or common origin.

Rheological analyses of clay suspensions with slightly higher contents of $1H_2O$-smectite and kaolinite lead to low-energy edge-to-edge or edge-to-face particle associations, non-Newtonian pseudoplastic behavior, maximum apparent viscosity of 180 Pa s at 0.008 s^{-1} followed by rapid descent. Clay fractions with higher $2H_2O$-smectite contents and lower kaolinite contents reach maximum viscosity of 3611 Pa s at a shear rate of 0.0018 s^{-1}, and 3300 Pa s at 0.0024 s^{-1}. They denote two high-energy probably face-to-face particle associations, followed by slow descent of the apparent viscosity under viscous flow. Suspensions change from elastic to viscous behavior, respectively, at shear stresses of 1.03 and 5.91 Pa. Clay suspension vibrated at a frequency of 1 Hz develops a shear storage dynamic modulus greater than the shear dynamic loss modulus or the energy is preferentially stored, whereas at 5 Hz more energy is dissipated than stored. The dynamic response of the clay fraction changes with the frequency of the applied vibration: at higher frequencies, energy tends to be dissipated whereas at low frequencies it tends to be stored.

The composition and behavior of the clay fractions in young basins, as in the Mexican Basin, is non-uniform and heterogeneous, across the sequence. Differences in swelling, physical, adsorption and chemical behaviors are expected. Depending on the abundance and distribution of clay in the bulk sediments, the behavior of the sediments will also be non-homogeneous.

ACKNOWLEDGMENTS

The authors acknowledge the financial support of the Consejo de Ciencia y Tecnologia and the National Science Foundation grant 400324-CO46A. They are indebted to the Dirección General de Construcción y Operación Hidraulica, Departamento del Distrito Federal, for supplying

material for study, and to A. Altamira, L. Cabrera, A. Maturano and M. Reyes for their contribution.

REFERENCES

Almon, W.R., Fullerton, L.B. and Davies, D.K. (1976) Pore space reduction in Cretaceous sandstone through chemical precipitation of clay minerals. *Journal of Sedimentary Petrology*, **46**, 89–96.

April, R.H. (1981) Trioctahedral smectite and interstratified chlorite/smectite in Jurassic strata of the Connecticut Valley. *Clays and Clay Minerals*, **29**, 31–39.

Bailey, S.W. (1988a) Structures and composition of other trioctahedral 1:1 phyllosilicates. Pp. 169–188 in: *Hydrous Phyllosilicates* (S.W. Bailey, editor). Reviews in Mineralogy, **19**. Mineralogical Society of America, Washington, D.C.

Bailey, S.W. (1988b) Chlorites: Structure and crystal chemistry. Pp. 347–404 in: *Hydrous Phyllosilicates* (S.W. Bailey, editor). Reviews in Mineralogy, **19**. Mineralogical Society of America, Washington, D.C.

Bailey, S.W. and Brown, B.E. (1982) Chlorite polytypism: I. Regular and semi-random one-layer structures. *American Mineralogist*, **47**, 819–850.

Barrenechea, J.F., Rodas, M., Frey, M., Alonso-Azcarate, J. and Mas, J.R. (2000) Chlorite, corrensite, and chlorite-mica in Late Jurassic fluvio-lacustrine sediments of the Cameros Basin of Northeastern Spain. *Clays and Clay Minerals*, **48**, 256–265.

Bettison-Varga, L. and Mackinnon, I.D.R. (1997) The role of randomly mixed-layered chlorite/smectite in the transformation of smectite to chlorite. *Clays and Clay Minerals*, **45**, 506–516.

Bodine, M.W. and Madsen, B.M. (1987) Mixed-layer chlorite/smectites from a Pennsylvanian evaporite cycle, Grand County, Utah. Pp. 85–93 in: *Proceedings of the International Conference, Denver* (L.G. Schultz, H. van Olphen and F.A. Mumpton, editors). The Clay Minerals Society, Bloomington, Indiana.

Brandenburg, U. and Lagaly, G. (1988) Rheological properties of sodium montmorillonite dispersions. *Applied Clay Science*, **124**, 624–631.

Brindley, G.W. (1982) Chemical composition of berthierine – a review. *Clays and Clay Minerals*, **30**, 153–155.

Chang, H.K., Mackenzie, F.T. and Schoonmaker, J. (1986) Comparisons between the diagenesis of dioctahedral and trioctahedral smectite Brazilian offshore basins. *Clays and Clay Minerals*, **34**, 407–423.

Chen, J.S., Cushman, J.H. and Low, P.F. (1990) Rheological behavior of Na-montmorillonite suspensions at low electrolyte concentration. *Clays and Clay Minerals*, **38**, 57–62.

Durazo, J. and Farvolden, R.N. (1989) The groundwater regime of the Valley of México from historic evidence and field observations. *Journal of Hydrology*, **112**, 171–190.

Furbish, W.J. (1975) Corrensite of deuteric origin. *American Mineralogist*, **60**, 928–930.

Gasca, D.A. and Reyes, C.M. (1977) *La cuenca lacustre Plio-Pleistocenica de Tula-Zumpango*. Instituto Nacional Antropologia e Historia, Informe **2**, 85 pp.

Güven, N. (1988) Smectites. Pp. 497–559 in: *Hydrous Phyllosilicates* (S.W. Bailey, editor), Reviews in Mineralogy, **19**. Mineralogical Society of America, Washington, D.C.

Heller, H. and Keren, R. (2001) Rheology of Na-rich montmorillonite suspension as affected by electrolyte concentration and shear rate. *Clays and Clay Minerals*, **49**, 286–291.

Hillier, S. (1993) Origin, diagenesis and mineralogy of chlorite minerals in Devonian Lacustrine mudrocks, Orcadian Basin, Scotland. *Clays and Clay Minerals*, **41**, 240–259.

Hillier, S. and Velde, B. (1991) Octahedral occupancy and the chemical composition of diagenetic (low-temperature) chlorites. *Clay Minerals*, **26**, 149–168.

Hoffman, J. and Hower, J. (1979) Clay mineral assemblages as low grade metamorphic geothermometers: application to the thrust faulted disturbed belt of Montana, USA. *Society of Economic Paleontology Mineralogy Special Publication*, **26**, 55–79.

Hower, J., Eslinger, E.V., Hower, M.E. and Perry, E.A. (1976) Mechanism of burial metamorphism of argillaceous sediments: I. Mineralogical and chemical evidence. *Geological Society of America Bulletin*, **87**, 727–737.

Hutcheon, I., Oldershaw, A. and Ghent, E.D. (1980) Diagenesis of Cretaceous sandstones of the Kootenay Formation at Elk Valley (southeastern British Columbia) and Mt. Allan (southwestern Alberta). *Geochimica et Cosmochimica Acta*, **44**, 1425–1435.

Inoue, A. and Utada, M. (1991) Smectite-to-chlorite transformation in thermally metamorphosed volcanoclastic rocks in the Kamikita area, northern Honshu, Japan. *American Mineralogist*, **76**, 628–640.

Jiang, W.T. and Peacor, D.R. (1994) Prograde transitions of corrensite and chlorite in low-grade pelitic rocks from the Gaspe Peninsula, Quebec. *Clays and Clay Minerals*, **42**, 497–517.

Jiang, W.T., Peacor, D.R. and Buseck, P.R. (1994) Chlorite geothermometry: Contamination and apparent octahedral vacancies. *Clays and Clay Minerals*, **42**, 593–605.

Karpova, G.V. (1969) Clay mineral post-sedimentary ranks in terrigenous rocks. *Sedimentology*, **13**, 5–20.

Kopp, O.C. and Fallis, S.M. (1974) Corrensite in the Wellington Formation, Lyons, Kansas. *American Mineralogist*, **59**, 623–624.

Kübler, B. (1973) La corrensite, indicateour possible de milleux de sedimentation et du degree de transformation d'un sediment. *Bulletin Centre Recherche Pau-SNPA*, **7**, 543–556.

Lopez-Ramos, E. (1979) *Geología de México, III*. Universidad Nacional A. de Mexico, Mexico.

Marsal, R.J. and Mazari, M. (1962) *El Subsuelo de la Ciudad de México*. Facultad de Ingenieria, Universidad Nacional A. de México, México.

Mering, J. and Pedro, G. (1969) Discussion a propos des criteres de classification des phyllosilicates 2:1. *Bulletin de Groupe Francaise Argiles*, **21**, 1–30.

Meunier, A., Clement, J., Bouchet, A. and Beaufort, D. (1988) Chlorite-calcite and corrensite-dolomite crystallization during two superimposed events of hydrothermal alteration in the 'les Cetes' granite, Vosge, France. *The Canadian Mineralogist*, **26**, 413–422.

Mooser, F. (1956a) *Vulcanismo y Rocas Sedimentarias Cuenca de México y Edo. De Morelos, Excursion C-9,* XX Congreso Geologico Internacional, Universidad Nacional A. de México, México.

Mooser, F. (1956b) *Informe sobre la Geología de la Cuenca del Valle de México,* Secretaria de Recursos Hidraulicos, Comision Hidrologica del Valle de México, México.

Moore, D.M. and Reynolds, R.C. (1997) *X-ray Diffraction and the Identification and Analysis of Clay Minerals*. Oxford University Press, New York.

Newman, A.C.D. (1987) The interaction of water with clay mineral surfaces. Pp. 241–260 in: *Chemistry of Clays and Clay Minerals* (A.C.D. Newman, editor). Mineralogical Society Monograph **6**. Longmans, Harlow, Essex, UK.

Newman, A.C.D. and Brown, G. (1987) The chemical constitution of clays. Pp. 49–63 in: *Chemistry of Clays and Clay Minerals* (A.C.D. Newman, editor). Mineralogical Society Monograph **6**. Longmans, Harlow, Essex, UK.

Odin, G.S. (1985) La 'verdine', facies granulaire vert, marin et cotier distinct de la glauconie: distribution actualle et composition. *Compte Rendue Academie Science Paris 301*, **2**, 105–108.

Odin, G.S., Bailey, S.W., Amouric, M., Frohlich, F. and Waychunas, G. S. (1988) Mineralogy of the verdine facies. Pp. 159–206 in: *Green Marine Clays* (G.S. Odin, editor). Developments in Sedimentology, **45**. Elsevier, Amsterdam.

Pevear, D.R. and Whitney, C.G. (1982) Clay minerals in Coast Range basalts of the Pacific Northwest: Eocene seafloor metamorphism. *Program with Abstracts, 19th Annual Meeting, Clay Minerals Society, Hilo, Haway,* p. 6.

Reynolds, R.C., Jr. and Reynolds, R.C., III (1996) *NEWMOD*: *The calculation of one dimensional X-ray diffraction patterns of Mixed-layered Clay Minerals. Computer Program.* 8 Brook Road, Hanover, New Hampshire 03755, USA.

Roberson, H.E. (1989) Corrensite in hydrothermally altered oceanic rocks. P. 59 in: *Abstracts of the 26th Clay Minerals Society Annual Meeting, Sacramento.*

Ruiz-Fernandez, A. (1999) *Distribucion espacial y temporal de metales pesados en sedimentos lacustres de la Cuenca de México: Chalco, Texcoco y Cuauhtitlan Izcalli, estado de México*. PhD thesis, Universidad Nacional A. de México, México.

Shau, Y.H., Peacor, D. and Essene, E. (1990) Corrensite and mixed-layer chlorite/corrensite in metabasalt from northern Taiwan: TEM/AEM, EPMA, XRD and optical studies. *Contributions to Mineralogy and Petrology*, **105**, 123–142.

Schiffman, P. and Staudigel, H. (1995) The smectite to chlorite transition in a fossil seamount hydrothermal system: The basement complex of La Palma, Canary Islands. *Journal of Metamorphic Petrology*, **13**, 487–498.

Sistema Hidraulico del Distrito Federal (1994) *Cronologia. Memoria de las Obras del Sistema de Drenaje Profundo del Dustrito Federal, Tomo I.* Departamento del Distrito Federal, México.

Suquet, H. and Pezerat, H. (1987) Parameters influencing layer stacking types in saponites and vermiculites. *Clays and Clay Minerals*, **35**, 353–362.

Suquet, H. and Pezerat, H. (1988) Comments on the classification of trioctahedral 2:1 phyllosilicates. *Clays and Clay Minerals*, **36**, 184–186.

Suquet, H., de la Calle, C. and Pezerat, H. (1975) Swelling and structural organization of saponite. *Clays and Clay Minerals*, **23**, 1–9.

Suquet, H., Iiyama, J.T., Kodama, H. and Pezerat, H. (1977) Synthesis and swelling properties of saponites with increasing layer charge. *Clays and Clay Minerals*, **25**, 231–242.

Urrutia-Fucugauchi, J., Lozano, S., Ortega, O., Caballero, M., Hansen, R., Bohnel, H. and Negendank, J.F.W. (1994) Paleomagnetic and paleoenvironmental studies in the southern Basin of México. I. Volcanosedimentary sequence and basin structure of Chalco lake. *Geofisica Internacional*, **33**, 421–430.

Van Olphen, H. (1977) *An Introduction to Clay Colloid Chemistry,* Interscience Publishers, New York.

(*Received 31 October 2001; revised 13 June 2002; Ms. 598; A.E. Ray E. Ferrell, Jr.*)